

Spatiotemporal Source Apportionment of Ozone Pollution over the Greater Bay Area

Yiang Chen ¹, Xingcheng Lu ^{2*} Jimmy C.H. Fung ^{1,3}

¹ Division of Environment and Sustainability, The Hong Kong University of Science and Technology, Clear Water Bay, Kowloon, Hong Kong SAR, China

² Department of Geography and Resource Management, The Chinese University of Hong Kong, Sha Tin, New Territory, Hong Kong SAR, China

³ Department of Mathematics, The Hong Kong University of Science and Technology, Clear Water Bay, Kowloon, Hong Kong SAR, China

Correspondence to: Xingcheng Lu (xingchenglu2011@gmail.com)

Abstract. It has been found that ozone (O₃) pollution episodic cases are prone to appear when the Greater Bay Area (GBA) is under the control of typhoons and sub-tropical high-pressure systems in summer. To prevent these pollutions effectively and efficiently, it's essential to understand the contribution of O₃ precursors emitted from different periods and areas under these unfavorable weather conditions. In this study, we further extended the Ozone Source Apportionment Technology (OSAT) from the Comprehensive Air Quality Model with Extensions (CAMx) model to include the function of tracking the emission periods of O₃ precursors. Subsequently, the updated OSAT module was applied to investigate the spatial-temporal contribution of precursor emissions to the O₃ concentration over the GBA in July and August 2016, when several O₃ episodic cases appeared in this period. Overall, the emissions within the GBA, from other regions of Guangdong province (GDo), and the neighbouring provinces were the three major contributors, accounting for 23%, 15%, and 17% of the monthly average O₃ concentration, respectively. More than 70% of O₃ in the current day was mainly formed from the pollutants emitted within 3 days and the same day's emission contributed approximately 30%. During the O₃ episodes, when the typhoon approached, more pollutants emitted 2-3 days ago from the GDo and adjacent provinces were transported to the GBA, leading to an increase in O₃ concentrations within this region. Under the persistent influence of northerly wind, the pollutants originating from eastern China earlier than 2 days ago can also show a noticeable impact on the O₃ over the GBA in the present day, accounting for approximately 12%. On the other hand, the O₃ pollution was primarily attributed to the local emission within 2 days when the GBA was mainly under the influence of the sub-tropical high-pressure systems. These results indicate the necessity to consider the influence of meteorological conditions in implementing the control measures. Meanwhile, analogous relationships between source area/time and receptor were derived by the zero-out method, supporting the validity of the updated OSAT module. Our approach and findings could offer more spatial-temporal information about the sources of O₃ pollutions, which could aid in the development of effective and timely control policies.

1. Introduction

As one of the major air pollutants, ozone (O₃) is a secondary pollutant formed by the photochemical reactions of nitrogen oxides (NO_x) and volatile organic compounds (VOCs) in the presence of solar radiation. Surface O₃ has detrimental effects on human health, such as causing respiratory and cardiovascular problems (Maji et al., 2019; Yin et al., 2017). It could also lead to the reduction of crop yield and the damage of vegetation (Gong et al., 2021; Wang et al., 2022c). With the implementation of a series of control policies in China since 2013, the concentrations of other air pollutants, including particulate matter with aerodynamic diameters less than 2.5µm (PM_{2.5}), NO_x, and sulfur dioxide (SO₂), have gradually decreased. In contrast, due to the large reduction of NO_x emission and limited control of VOCs emission in the early stage of the control period (Liu et al., 2023), the O₃ concentration still continuously increased and has become the primary air pollutant across China. The Greater Bay Area (GBA), including nine cities in the Pearl River Delta (PRD) region, Hong Kong (HK), and Macau Special Administrative Regions (SAR), is one of the most developed agglomerations in China and also faces the heavy O₃ pollution problem. Based on the analysis of surface monitor observation, Cao et al. (2024) and Feng et al. (2023) revealed

48 an overall upward trend in the maximum daily 8-h average (MDA8) O₃ in the PRD region and HK, with an
49 increase of 1.11 and 0.22 ppbv/year from 2013 to 2019 and from 2011 to 2022, respectively.

50 The formation of O₃ is closely related to the sources of its precursors, and much effort has been devoted to
51 investigating the source region and source category of O₃ in the GBA using different methods (Liu et al., 2020a).
52 He et al. (2019) applied the positive matrix factorization (PMF) method to resolve the anthropogenic sources of
53 VOCs. Combining a photochemical box model with the master chemical mechanism (PBM-MCM), they found
54 that vehicular was the most significant source of the O₃ formation, followed by biomass burning and solvent usage.
55 Li et al. (2012) applied the CAMx-OSAT numerical model to track the source contribution to O₃ in the GBA
56 region and found that elevated local and regional contributions were dominant during the O₃ episodes. Yang et al.
57 (2019b) applied the NAQPMS model with an online source apportionment module to explore the sources of O₃
58 in different seasons in the PRD region. Their results showed that the mobile was the largest contributor, followed
59 by industry. Fang et al. (2021) used multi-modelling source apportionments to quantify the source impact on O₃
60 in the PRD region. The on-road mobile and industrial process were found to be two major contribution sectors.
61 Integrating satellite data and sensitivity model simulations, Wang et al. (2022a) found that enhanced biogenic
62 emission and cross-regional transport due to approaching typhoons were significant factors leading to ozone
63 pollution in the PRD and Yangtze River Delta (YRD) regions. In addition to the source region and category, the
64 emitting time of pollutants is also an important perspective that needs a better understanding for effective and
65 efficient control policymaking. Several studies have attempted to evaluate this temporal perspective (Xie et al.,
66 2021; Ying et al., 2021). Xie et al. (2023) analysed the age evolution of PM_{2.5} during a haze event in eastern China.
67 It showed that during the regional transport stage, more aged particles from the North China Plain (NCP) were
68 transported to the downwind YRD region, leading to a sharp increase in the average age of different components
69 of PM_{2.5} in the YRD. Chen et al. (2022c) investigated the temporal contributions of emissions to the concentration
70 of PM_{2.5} in the PRD region and found that pollutants emitted 2 days earlier were trapped within the PRD region
71 due to the weak wind during the episodic pollution. However, these studies mainly focused on the PM_{2.5} and the
72 temporal contribution of sources to the O₃ in the GBA region still remains unclear.

73 In addition to emission, meteorological conditions, another key factor that can affect the transportation,
74 production, and destruction of O₃ and its precursors, have also received much attention and have been extensively
75 studied (Lu et al., 2019; Wang et al., 2017; 2022b). The long/short-term effects of meteorological changes on
76 ozone concentrations have been investigated through various methods, such as statistical analysis of observations
77 and numerical modelling (Yang et al., 2019a; Xu et al., 2023a; Zheng et al., 2023). Liu and Wang (2020b)
78 conducted sensitivity simulations by the CMAQ model to evaluate the contribution of variations in weather
79 conditions to summer O₃ levels from 2013-2017. Their results showed that the meteorological conditions were
80 more conducive to ozone formation from 2014 to 2016 than in 2013, leading to an increase of more than 10 ppbv
81 in MDA8 O₃ in Guangzhou. Different objective and subjective classification technologies have been applied to
82 summarize the impacts of unfavorable weather patterns on O₃ pollution (Han et al., 2020; Chen et al., 2022b; Cao
83 et al., 2023). Gao et al. (2018) summarized the common synoptic patterns in the Guangdong province that O₃
84 pollution always occurred and concluded that the sub-tropical high-pressure system and typhoons are two major
85 patterns accounting for more than 60% of cases in the PRD regions during 2014 - 2016. The major influencing
86 factors and the dominant physical and chemical processes were also identified and analyzed (Gong et al., 2022;
87 Zeren et al., 2022; Wu et al., 2023). Ouyang et al. (2022) analysed the impact of a subtropical high and a typhoon
88 on ozone pollution in the PRD region and found that low relative humidity, high boundary layer height, weak
89 northerly surface wind, and strong downdrafts were the main meteorological factors contributing to the pollution.
90 Deng et al. (2019) illustrated that the actinic flux was the important cause of the co-occurrence of high ozone and
91 aerosol pollution under the control of typhoon periphery. Li et al. (2022) also investigated the impact of peripheral
92 circulation characteristics of typhoons and found that the chemical formation and vertical mixing effects were two
93 major contributors to the enhancement of O₃ levels, while the advection showed negative values. Qu et al. (2021)
94 analysed the typhoon-induced and non-typhoon O₃ events in the PRD region and revealed that under the influence
95 of typhoons, the contributions from the transport processes and sources outside the PRD increased. Usually, the
96 ozone events are attributed to changes in meteorological conditions rather than sudden increases in emission
97 intensity (Lin et al., 2019; Xu et al., 2023b). The changes in weather conditions will affect the time-sensitivity of
98 emitted pollutants and lead to different types of O₃ pollution, such as long-range transport of aged pollutants or
99 accumulation of local fresh pollutants. Hence, it is of great importance to clarify the impact of the pollutants from
100 different source areas and emitting periods on the O₃ pollution under different weather conditions in the GBA.
101 In this study, the CAMx-OSAT model was extended and used to track the temporal contribution of pollutants to
102 the O₃ pollutions over the GBA under the impact of typhoons and sub-tropical high pressure during July and

103 August in 2016, the two most important weather systems that influence O₃ pollutions over the GBA. The rest of
 104 this paper is organized as follows. The temporal source apportionment (TSA) method, the configuration of
 105 experiments, and the ozone episodes are introduced in section 2. The spatial-temporal source apportionment
 106 results and zero-out simulation results are shown and discussed in section 3. The major conclusions are
 107 summarised in section 4.

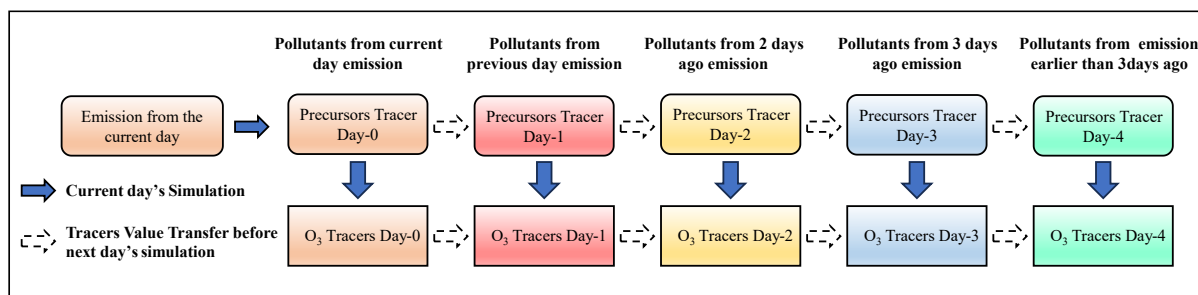
108

109 2. Methodology and Data

110 2.1 Temporal Source Apportionment Method

111 Previously, we have successfully implemented the PM_{2.5} temporal source apportionment method in the CAMx
 112 model and applied it to investigate the temporal influence of emissions on PM_{2.5} in the GBA (Chen et al., 2022c).
 113 Here, we further extend this method to track the temporal contribution of emissions to the precursors and the
 114 formation of O₃. Similar to the OSAT method, the input data used in the TSA method developed in this work
 115 include the source area map and hourly emission data. The source area map assigns each model grid cell to one
 116 of the specific source regions. The hourly emission data is the same as the one used in the normal CAMx model
 117 simulation without turning on the source apportionment module. The basic mechanism of the TSA method is to
 118 track the contribution of pollutants from different emitting periods using a set of tracers. In the TSA method (Fig.
 119 1), the *Precursor Tracer Day-x* was used to track the precursors emitted from *x* days ago. The *O₃ Tracer Day-x*
 120 was used to track the O₃ formed from the precursors emitted from corresponding *x* days ago (namely *Precursor*
 121 *Tracer Day-x*). The tracers in *Day-x* can be set into different finer periods (e.g., every 1 hour, 6 hours, 24 hours)
 122 as required. The total number of tracers will be decided according to the entire tracking period and the minimum
 123 tracking period per tracer. For instance, if the entire tracking period is 5 days and the minimum tracking period
 124 per tracer is every 6 hours, the total number of tracers will be 20. In each time step, the tracers go through all the
 125 processes, including emission, transport, diffusion, and chemical reactions, sequentially, as in the normal CAMx
 126 model simulation. Therefore, the precursors and O₃ tracers that tracked different periods are calculated
 127 simultaneously. When the pollutants emitted from the sources, they will be assigned to the *Precursor Tracer* in
 128 *Day-0*, while the *Precursor Tracers* that tracked other periods and the *O₃ Tracers* remain unchanged. The data
 129 transfer between tracers (e.g., *Day-1* to *Day-2*, and *Day-0* to *Day-1*, dash arrow in Figure 1) will be conducted
 130 once after one day's simulation. As shown in Figure 1, during each day's simulation, the contribution of the present
 131 day's emission is consistently tracked by the *Day-0* tracers. After completing the current day's simulation and
 132 before starting the next day's simulation, each tracer *Day-x*'s value transfers to the corresponding tracer *Day-(x+1)*,
 133 which represents one day earlier than *Day-x*, following the specified sequence. For example, beginning from the
 134 penultimate tracer, namely values in *Day-3* transfer and add into *Day-4*, then the values in *Day-2* transfer to *Day-3*,
 135 followed by *Day-1* to *Day-2*, and lastly *Day-0* to *Day-1* (Dash arrow in Figure 1). Here, the value in *Day-3*
 136 tracer will be added into the last tracer (*Day-4*) because the last tracer represents the total contribution of pollutants
 137 emitted earlier than 3 days ago. Same as the OSAT method, the TSA method also utilizes the photochemical
 138 indicator, namely, the ratio of the production rate of hydrogen peroxide (H₂O₂) and nitric acid (HNO₃), to
 139 determine the sensitivity of O₃ formation. When the O₃ formation is classified as NO_x-limited (VOC-limited), the
 140 contributions are distributed to the NO_x (VOCs) sources emitted at different periods, based on the proportion of
 141 their emissions to the total NO_x (VOCs) emissions. More details of this method can be found in Chen et al. (2022c).

142



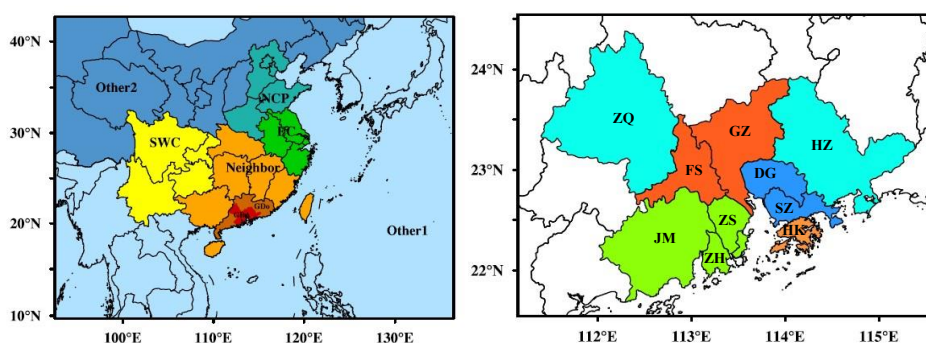
143 Figure 1. Schematic diagram of temporal source apportionment (colors represent the pollutants released or formed
 144 by emissions on different days).

145

146 **2.2 Model Configuration and Evaluation**

147 The Weather Research and Forecasting (WRFv3.9) model was applied for meteorological field simulation. The
 148 initial and boundary condition for the WRF model was gained from the Final Operational Global Analysis data
 149 (FNL). The CAMx v7.1 was used to simulate the spatial-temporal variation of air pollutants. The initial and
 150 boundary condition for the CAMx model was provided by the Model for Ozone and Related chemical Tracers,
 151 version 4 (MOZART-4). Regarding the emission, a highly resolved emission inventory provided by the Hong
 152 Kong Environmental Protection Department (HKEPD) was used for the GBA region, and the Multi-resolution
 153 Emission Inventory for China (MEIC, Li et al., 2017) developed by the Tsinghua University was applied for the
 154 area outside the GBA region. The biogenic emission for the entire domain was calculated by the Model of
 155 Emissions of Gases and Aerosols from Nature (MEGAN version 3.1). The CB05 gas phase chemistry, the
 156 ISORROPIA inorganic aerosol scheme, and the SOAP secondary organic aerosol scheme were used in the
 157 simulation. This model system has been applied to analyse the source of O₃, NO_x, and PM_{2.5} in the GBA region in
 158 previous studies (Lu et al., 2016; Chen et al., 2022a; Chen et al., 2022c). More configuration of this model system
 159 can refer to the work of Lu et al. (2016).

160 The three-nested simulation domain of the WRF-CAMx model was shown in Figure S1. The resolution of three
 161 domains was 27km, 9km, and 3km, respectively. For the source apportionment experiments, the simulation
 162 domain was divided into 12 source regions as shown in Figure 2, including North China Plain (*NCP*), eastern
 163 China(*EC*), southern western China (*SWC*), other regions of inland China (*Other 2*), ocean and other countries
 164 (*Other 1*), neighbouring provinces around Guangdong province (*Neighbor*), Other region within Guangdong
 165 province but outside the GBA(*GDo*), different sub-regions within the GBA: Guangzhou and Foshan(*GF*),
 166 Shenzhen and Dongguan(*SD*), Hong Kong (*HK*), Zhuhai, Zhongshan and Jiangmen (*ZZJ*), Zhaoqing and
 167 Huizhou(*GBAo*). The cities within the GBA were separated into different sub-regions mainly based on
 168 administrated boundaries and their geographical location, same as the work of Chen et al. (2022c). The sub-regions
 169 mainly consist of neighboring cities. Zhaoqing and Huizhou, located at the northwestern and northeastern corners,
 170 respectively, were categorized into one group since they have a relatively lower emission density than other cities.
 171 Previous studies indicated that the air pollutants in Hong Kong were usually more influenced by long-range
 172 transport from regions outside the GBA, in contrast to the other cities in the GBA (Li et al., 2012; Chen et al.,
 173 2022a; Chen et al., 2022c). Hence, Hong Kong city is treated as a separate entity. The contribution of initial and
 174 D1 boundary conditions were also treated as two sources. In the following analysis, for the O₃ concentrations in
 175 the target area over the GBA, the influence of pollutants emitted within the target area is treated as the local
 176 contribution, and the influence of pollutants originating from the other areas within the GBA region is treated as
 177 the regional contribution. The source tracking time period is 5 days. Day-0, Day-1, Day-2, Day-3 represent the
 178 pollutants emitted within the present day, the previous day, two days ago, and three days ago, respectively. Day-4
 179 represents the total contribution of pollutants emitted earlier than three days ago. The simulation period is July
 180 and August 2016, and the model was spin-up for 7 days to reduce the influence of initial condition.



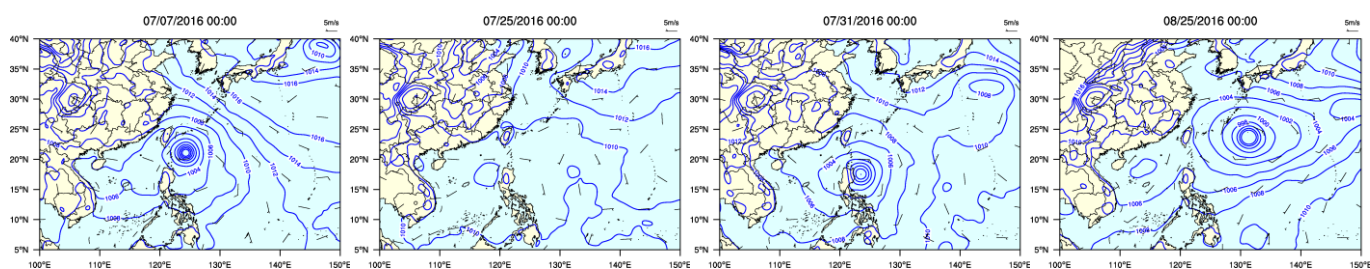
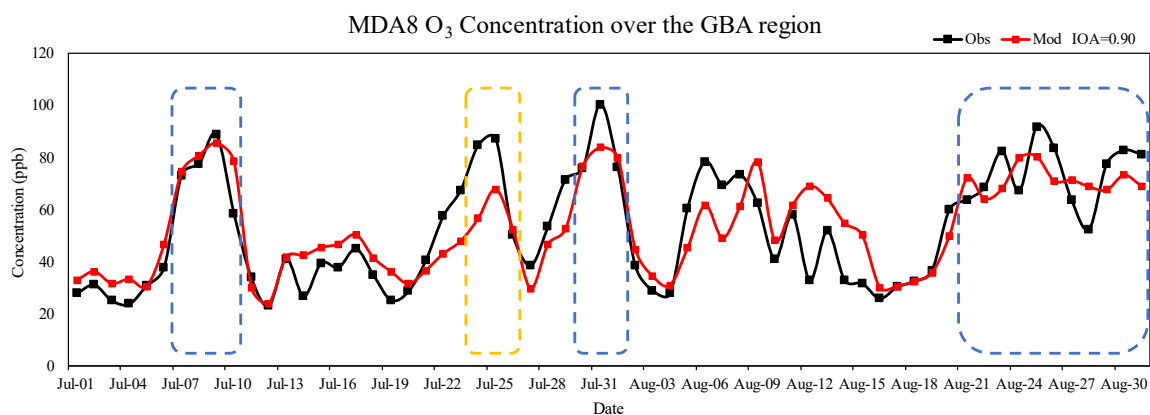
181
 182 Figure 2. The configuration of source areas in the source apportionment experiments (One color represents one
 183 source area. The GBA source were divided into five source areas. *Other 1* represents ocean and other countries.
 184 *Other 2* represents other area within the mainland China in the simulation domain.)

185 The performance of simulated hourly 2-m temperature, 10-m wind speed, and O₃ concentration were evaluated
 186 and shown in Table S1. Here, the statistical metrics, including mean bias (MB), normalized mean bias (NMB),
 187 index of agreement (IOA), and root mean square error (RMSE), were used for model performance evaluation.
 188 The mathematical formulas for these metrics can be found in Table S6. The recommended values suggested by

189 Emery et al. (2001) and EPA (2007) were used as benchmarks and shown in the brackets in Table S1. The
190 temperature is a little overestimated with a MB of 0.33, while the wind speed is underestimated with a MB of -
191 0.45. The IOA is 0.82 and 0.70 for temperature and wind speed, respectively. The MBs and IOAs both fulfill the
192 criteria. But the RMSE shows a little higher than the value of criteria. Regarding the O₃, the IOA reaches 0.81.
193 The small positive MB indicates that the model slightly overestimates the O₃ concentration. The NMB is 0.13,
194 which also meets the criteria. The time series comparison (Fig. S2) of average O₃ concentration in Guangzhou,
195 Hong Kong and Zhuhai illustrates that the model can well catch and reproduce the variation trend of O₃
196 concentration in GBA, although there are a few differences between the simulated and measured concentration
197 for some peaks, like the period between 25 July and 31 July in Guangzhou. Overall, the performance of model
198 simulation is comparable to the other studies in this region (Li et al. 2022; Yang and Zhao, 2023). Therefore, the
199 simulation result is reasonable and can be further used for source analysis.

200 **2.3 Ozone Episodes**

201 There were several O₃ episodes that occurred during the simulation period. Here, the maximum daily 8-h average
202 (MDA8) O₃ concentration over the GBA was calculated using the observation data from the surface monitors
203 stations (Fig. 3). The O₃ observations were obtained from the China National Environmental Monitoring Centre
204 (CNEMC) and the HKEPD. Here, pollution days were identified when the average MDA8 O₃ observations
205 concentrations over the GBA exceeded 80ppb (Wang et al., 2022d). To better capture the evolution of the O₃
206 pollution, based on the characteristics of concentration variation, the days preceding and following the O₃
207 pollution days were also included in the analysis and the whole period was considered as an O₃ episode. The first
208 O₃ pollution occurred between the 7th and 10th of July (Ep1). During this period, the GBA region was initially
209 controlled by the sub-tropical high-pressure system. When the typhoon north-westerly moved from the east sea
210 area of the Philippines towards Taiwan province, the GBA was located in the peripheral subsidence region. After
211 the typhoon made landfall, the high-pressure situation in the GBA was relieved and the O₃ concentration decreased.
212 There were another two O₃ episodes between 24 July and 1st August. The GBA was mainly influenced by the sub-
213 tropical high-pressure system during 24th-26th July (Ep 2), while the synoptic condition of the GBA between 30th
214 July-1st August (Ep3) was similar to that of Ep1. During the Ep3, another typhoon moved north-westerly from
215 the east sea area of the Philippines and influenced the GBA region. It was found that this type of typhoon
216 movement path was often accompanied by the occurrences of O₃ pollution in the GBA (Wang et al., 2022a). In
217 late August, under the joint influence of the subtropical high-pressure system and the typhoon, the O₃ over the
218 GBA maintained a high concentration level between the 21st -31st of August (Ep4). Unlike previous two typhoons,
219 this typhoon moved southerly from the sea areas south of Japan and stayed near the sea areas east of Taiwan
220 province. The typhoon moved northwards after 27th August, and northerly winds prevailed in the GBA. Hence,
221 we conducted the simulation of O₃ concentration in the GBA during July-August 2016 and analysed the
222 spatiotemporal contributions of emissions in these episodic cases.



223

224 Figure 3. The time-series of the observed and simulated MDA8 O₃ concentration over the GBA during July-
 225 August 2016 and the synoptic patterns during the O₃ episodes. (Blue box: typhoon case; Yellow box: sub-
 226 tropical high-pressure case. The O₃ observations were obtained from the CNEMC and the HKEPD. The
 227 synoptic patterns were plotted using the ERA5 reanalysis data)

228

229 3. Result and Discussion

230 3.1 Source Area Contributions

231 The contribution of different source areas to the average hourly O₃ concentration in the GBA region is shown in
 232 Table 1. Here, the contribution from initial and boundary conditions were treated as background contribution.
 233 Regarding the monthly average O₃ concentration over the GBA region, the emission within the GBA can
 234 contribute about 23%. The pollutants from other regions within Guangdong Province (GDo) and neighbouring
 235 provinces also had large contribution, accounting for approximately 15% and 17%, respectively. Under the
 236 influence of prevailing south winds in the summertime, the contribution from ocean and other countries can also
 237 account for about 20%. As some studies suggested that O₃ originating from foreign countries is quite limited (Sahu
 238 et al., 2021), the main contributor of this source is likely to be marine ship emissions from ocean. The pollutants
 239 from other source regions had limited effect on the O₃ in the GBA.

240 The monthly average source area contribution to four sub-regions within the GBA region can be found in Table
 241 S2. Results show that the local emission had a significant influence on O₃ in the GF and SD regions, accounting
 242 for 17% of O₃ but its impact was lower than 10% on O₃ in the ZZJ region and HK city. The contribution of GBA
 243 regional emissions (contributed by other GBA tagged regions) had a relatively larger impact on the monthly
 244 average O₃ concentration in the GF region than the other sub-regions. It's because of the prevailing southerly wind
 245 in summer, which resulted in a greater influence of the pollutants within the GBA region on O₃ in the GF area.
 246 The influences of pollutants from GDo and neighboring provinces on different subregions ranged from 25% to
 247 31%. As coastal regions, the ZZJ region and HK city were also more affected by sources of ocean and other
 248 countries, which occupied about 24% and 27%, respectively.

249 Regarding the average hourly O₃ concentration over the GBA region in different episode periods, it can be found
 250 that, during the typhoon episodes (i.e., Ep1, Ep3 and Ep4), the contribution of non-local emission has increased.
 251 The typhoon paths were quite similar in the Ep1 and Ep3 episodes (Fig. S3). Results show that the total
 252 contribution of GDo and neighbouring provinces have increased and reached more than 50% for O₃ over the GBA
 253 in these two typhoon episodes. As shown in Figure S4, with the approaching of the typhoon, the wind speed

254 increased and the average wind direction over the GBA changed from south to north. Therefore, more pollutants
 255 from the surrounding provinces were transported to the GBA. Considering the typical circulation patterns of the
 256 typhoon periphery (Figure. S4 and S6), it is inferred that more pollutants may come from Jiangxi, Fujian, and
 257 Hunan provinces. During the Ep1 and Ep3 episodes, the contribution of local emission in different sub-regions
 258 slightly decreased. With the change of the wind direction from south to north in these two periods, the influence
 259 of pollutants within the GBA to O₃ in the GF area decreased from 15% to 8%. The contribution of the GBA
 260 emission to the O₃ in other sub-regions increased, especially the ZZJ area and HK city. It is because of the change
 261 of wind direction, these two regions were located at the downwind area of the GF and SD regions, which are the
 262 emission hotspots within the GBA. At the same time, the contribution of source from ocean and other countries
 263 also decreased by approximately 10%. The contribution of emission from the GDo and neighboring provinces to
 264 O₃ concentration in GF, SD, ZZJ regions, and HK city increased by 27%, 21%, 32%, and 22%, respectively.

265 In another typhoon process (Ep4), where the typhoon's moving path differed from the other two typhoon cases,
 266 an increase in the contribution from GDo and neighbouring provinces was observed due to the persistent northerly
 267 winds. Furthermore, it was observed that pollutants from eastern China (EC) and North China Plain (NCP) could
 268 also influence the O₃ levels in the GBA, accounting for approximately 12%. Similar increases in the impact of
 269 emissions from the EC and NCP were also found in the four sub-regions.

270 In the Ep2, the GBA was mainly controlled by the sub-tropical high-pressure system, with prevailing southerly
 271 wind. However, the low wind speed was conducive to the accumulation of the pollutants. Hence, the local sources
 272 were the dominant contributors and accounted for about 44%, while the contribution from GDo and neighboring
 273 provinces decreased. For O₃ in the GF region, as discussed above, the O₃ in the GF region is more susceptible to
 274 emissions within the GBA under the prevailing southerly wind. Thus, not only the local contribution but also the
 275 GBA regional contribution largely increased in the GF region. The regional contribution is larger in the GF region,
 276 increasing from 15% to 33%. On the other hand, the main increase in other sub-regions was seen in the local
 277 contributions.

278

279 Table 1. Contribution of pollutants from different source areas to the average hourly O₃ concentration over the
 280 GBA in different cases.

Case	GBA	GDo	Neighbor	Other 1	EC	SWC	NCP	Other 2	Background
Monthly	23%	15%	17%	20%	3%	1%	1%	1%	20%
Ep1	18%	21%	35%	10%	3%	0%	0%	0%	13%
Ep2	44%	11%	7%	27%	0%	0%	0%	0%	11%
Ep3	19%	34%	25%	9%	3%	0%	1%	1%	9%
Ep4	20%	16%	18%	15%	8%	1%	4%	3%	14%

281 * Here, *GDo* represents areas outside the GBA but within Guangdong province. *Neighbor* represents the provinces around
 282 Guangdong province. *Other 1* represents ocean and other countries. *Other 2* represents other areas within the mainland China
 283 in the simulation domain. *Background* represents the contribution of initial and boundary conditions.

284 3.2 Emission Period Contributions

285 The contribution of pollutants emitted from different time periods to the average hourly O₃ concentration in the
 286 GBA and its sub-regions is shown Figure 4 and Table S3. The background contribution was not considered in the
 287 temporal source contribution analysis. This is because the background contribution is primarily derived from
 288 boundary conditions, and its temporal contribution is calculated based on the time when the pollutants are
 289 transported into D1, rather than the actual emission time.

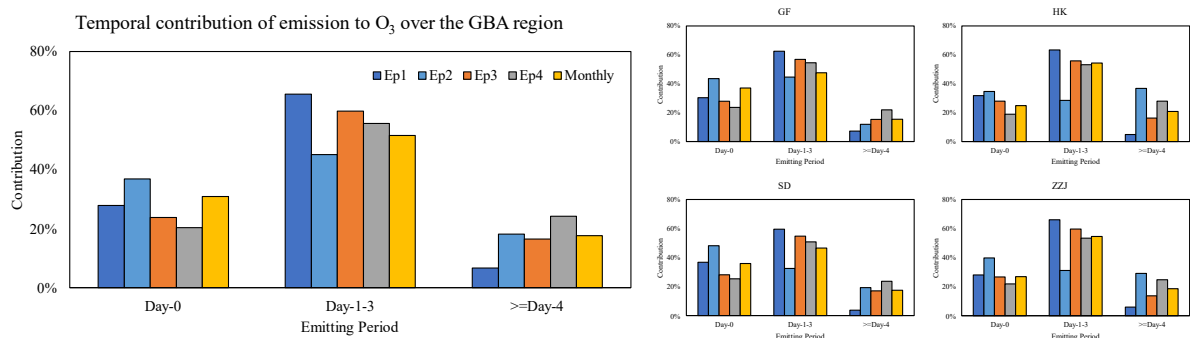
290 Overall, under the general monthly condition, the emissions within 3 days (namely from Day-0 to Day-2) account
 291 for approximately 73% of the monthly average O₃ concentration within the GBA. The largest proportion of O₃,
 292 around 31%, was formed from the current day's emission (Day-0) and the contribution of pollutants from earlier
 293 emission periods decreased as time elapsed. For the monthly average O₃ in different sub-regions, more O₃ in the
 294 GF and SD regions was formed from the emission from Day-0, which contributed about 37% and 36%,
 295 respectively. The contribution of emissions from Day-1 decreased to about 23% in these two regions. The
 296 contribution of Day-0 and Day-1 emissions was relatively small but stable for the HK city and ZZJ region, which

297 accounted for around 25% and 27%, respectively. The influence of pollutants emitted earlier than 3 days ago (i.e.,
 298 Day-4) was generally lower than 20%.

299 The situations are different during the pollution periods. The contribution of emission from the current days to the
 300 average hourly O₃ over the GBA both decreased in the two typhoon cases with similar moving paths (Ep1 and
 301 Ep3). However, the contribution of emissions from Day-1 to Day-3 increased 14% and 8%, respectively. And the
 302 influence of pollutants emitted earlier than 3 days ago (Day-4) decreased 11% in Ep1 and remained almost
 303 unchanged in Ep3. These findings indicate that these two ozone pollutions were caused by the accumulation of
 304 pollutants within the current 3 days.

305 For another typhoon case (Ep4), the contribution from Day-0 decreased approximately by 11%, compared to the
 306 monthly contribution over the GBA. At the same time, the influence of pollutants from earlier emitting periods
 307 increased, especially for those emitted earlier than 3 days ago. It means that the O₃ pollution during this period
 308 was a persistent pollution process. The major contributor should involve not only local emissions but also long-
 309 range transport. Similar trends in temporal contribution variations were observed in different sub-regions, which
 310 also illustrated that O₃ pollution is usually a regional problem.

311 For Ep2, the contribution of emissions from Day-0 increased approximately 18%, while the influence of emissions
 312 from Day-1 to Day3 decreased about 18%. According to the source area contribution result, the source area of O₃
 313 over GBA in Ep2 is mainly local sources. Therefore, the contribution of freshly emitted pollutants was larger. The
 314 contribution of Day-4 emissions to the HK city and ZZJ region in Ep2 was larger. It is probably because of the
 315 prevailing south wind direction, which brought more airflow from the ocean. Compared with the emission of the
 316 GF and SD regions, the HK city and ZZJ region have lower emission amounts. At the same time, HK city and
 317 ZZJ region were located in the upwind region, and the pollutants from GBA would have a smaller influence on
 318 the O₃ in these two regions. Hence, the amount of fresh pollutants was smaller and contributed similarly to Day-
 319 4 emissions, which is an accumulated amount.



320
 321 Figure 4. Contribution of pollutants from different emitting periods to the average hourly O₃ concentration over
 322 the GBA in different cases.

323
 324 **3.3 Source Area-Time Contributions**

325 To further clarify the relationship between sources and the O₃ concentration in target regions, the evolution of O₃
 326 from various source areas and periods was analyzed. Figure 5 shows the time series of the contributions from
 327 different source areas and precursor emission periods to the hourly average O₃ concentration in the GBA region.

328 Regarding the monthly average O₃ concentration over the GBA, the emission within the GBA was the major
 329 contributor and generally had a larger effect on the current day. Under the control of southerly wind, as shown in
 330 Figure 6, the pollutants emitted 1 day ago (Day-1) were gradually transported out of the GBA, and the influence
 331 of the GBA's emission earlier than Day-1 diminished. Simultaneously, the pollutants of GDo and neighboring
 332 provinces emitted 1 day ago began to have an impact on the O₃ in the GBA. However, due to the prevailing
 333 southerly wind, the impact of aged pollutants from GDo and neighboring provinces on the O₃ in the GBA was
 334 relatively low.

335 However, regarding the O₃ pollution between 7th and 10th July (Ep1), the major contributors changed. On 7th July,
 336 the GBA was under the control of the subtropical high-pressure system, and the typhoon was located near the east

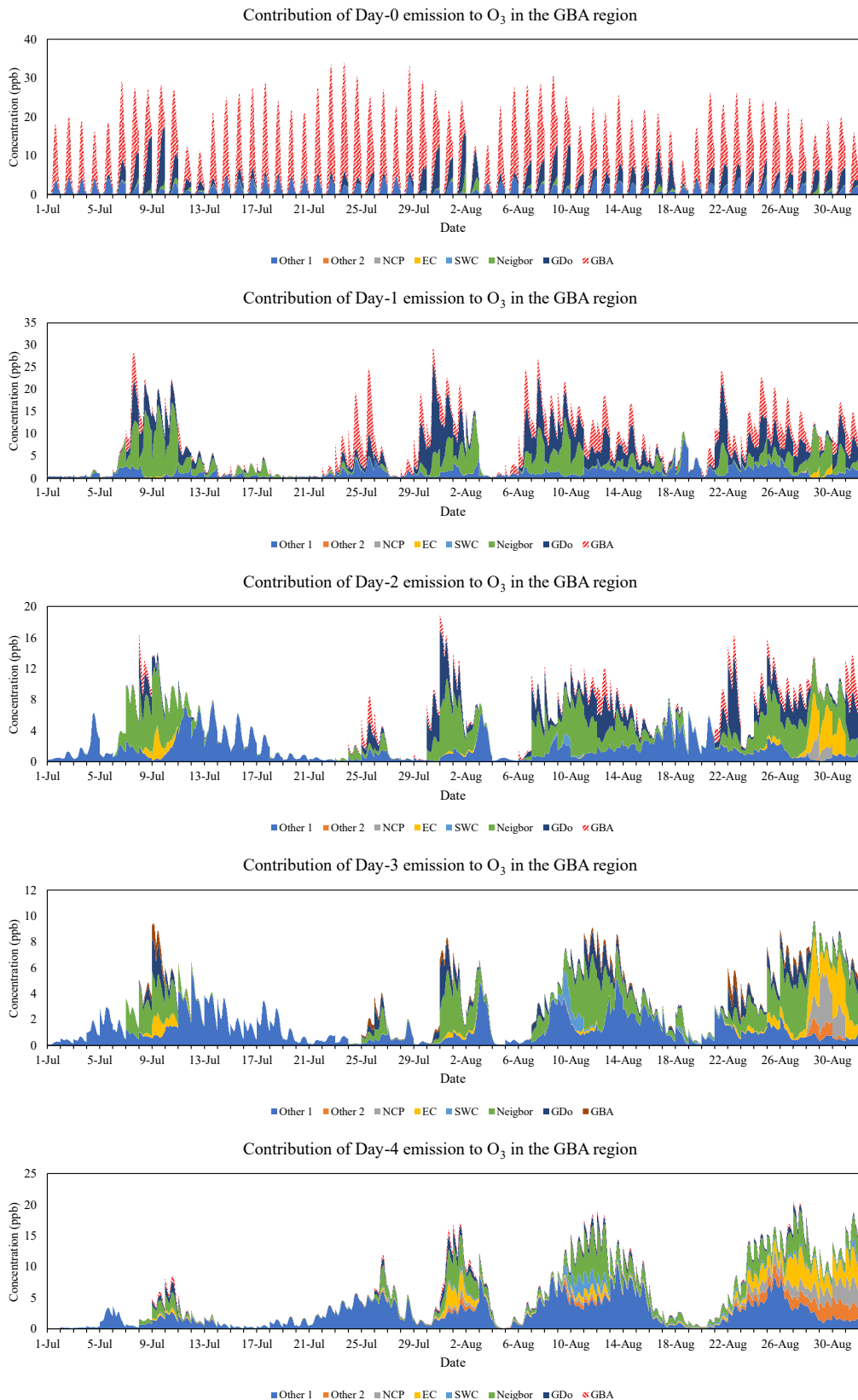
337 of Taiwan province. The weather condition was unfavourable for pollutants dispersion, and the O₃ sourced from
338 Day-1 emission within Guangdong provinces was trapped. The prevailing wind shifted to northerly wind, bringing
339 elder pollutants from neighboring provinces to the GBA. With the approach of the typhoon from 8th–10th July,
340 the stronger northwest wind speeded up the diffusion of pollutants from the GBA and decreased the local
341 contribution. However, it also transported more elder pollutants from the northern inland to the GBA. It can be
342 found that the emissions from GDo on the present day also had a significant contribution. At the same time, the
343 pollutants from the neighboring provinces dominated the emissions from Day-1 to Day-3. Moreover, the
344 pollutants emitted 2 days ago in the EC were also transported southward and affected the O₃ in the GBA on the
345 current day. Figure 7 shows the spatial distribution of the average source contribution during the Ep1 period.
346 Compared with the monthly average (Figure 6), it was found that the elder pollutants originating from the GBA
347 can be transported back and influence the O₃ concentration in the western part of the GBA during the Ep1 period.
348 This is because easterly winds blew over the GBA from 5th–6th July (Before Ep1, Figure S4). The pollutants emitted
349 within the GBA were transported to northwest inland. However, under the influence of northwest wind, they were
350 transported back to the GBA again. It can also be seen that the pollutants from the GDo 1 day ago were transported
351 downwind quickly, contributing to a high O₃ concentration over the Pearl River Estuary. According to the wind
352 pattern, they mainly came from the northern and western parts of the Guangdong province. Meanwhile, the
353 neighboring provinces' emissions from Day-1 to Day-3 were also transported to the GBA by the northwest wind,
354 continuously affecting the O₃ over this region.

355 For the Ep3 O₃ pollution process, results show that the pollutants from GDo and neighboring provinces were also
356 the major contributors. From 30th–31st July, the GBA was under the control of high pressure, and weak north wind
357 prevailed in this region. Afterward, the approaching of the typhoon (1st August) further strengthened the cross-
358 regional transport of pollutants. The difference between Ep3 and Ep1 is that the emissions from GDo have a larger
359 proportion in the Day-1 and Day-2 emissions. Additionally, while pollutants from neighboring provinces and EC
360 in Day-4 emission only accounted for about 5ppb in Ep1, they can still contribute to about 10ppb in Ep3. The
361 possible reason is that northerly wind prevailed over Fujian, Jiangxi, and Hunan provinces during the whole Ep1
362 period (Figure S4). However, easterly wind still blew over these provinces during the earlier period of the Ep3
363 (30th–31st July, Figure S6), which slowed the transport and influence of pollutants from the neighboring provinces.
364 Generally, the pathways of typhoons in the Ep1 and Ep3 episodes were quite similar, and the influence regions of
365 typhoon wind field mainly covered Guangdong and neighboring provinces. Therefore, the major source area and
366 source time were quite similar in these two cases. To prevent this type of O₃ pollution, earlier emission control (at
367 least 3 days ago) and collaboration with neighboring provinces will gain a better control result.

368 On the other hand, the situation is different for the Ep2 ozone pollution. Under the control of the high-pressure
369 system and weak southerly wind (Figure S5), the major contributors were mainly the pollutants from the GBA
370 and the ocean. Unlike the Ep1 and Ep3, the pollutant emitted within the GBA was still dominant in the contribution
371 of Day-1's emission. Under the influence of southerly wind, there was minimal migration of pollutants from north
372 inland regions to the GBA, and the local pollutants were gradually dispersing from the GBA. Thus, the pollutant
373 emitted earlier than 2 days ago (\geq Day-2) had a smaller contribution. As shown in Figure 8, the overall diffusion
374 of pollutants within the Guangdong province was much slower during Ep2. The contribution of the GBA emissions
375 can still reach more than 10 ppb in the Day-1 emission. These results indicate that this pollution process was
376 mainly driven by the local pollutants within the current 2 days. Hence, emission control should focus on the local
377 sources, and 1-2 days in advance is more efficient.

378 For the last O₃ pollution process (Ep4), which occurred from the 21st to 25th August, eastern and southern China
379 were mainly controlled by the sub-tropical high-pressure system. Meanwhile, under the joint influence of
380 peripheral subsidence airflow of typhoon, the wind speed over this region was slow (Figure S7). The weak wind
381 not only trapped the O₃ formed from local emission but also the O₃ formed from cross-regional transported
382 pollutants. The pollutants from the GBA sources mainly dominated the Day-0 and Day-1 emission's contribution,
383 while Day-2 and Day-3 emissions mainly consisted of pollutants from GDo and neighboring provinces.
384 Subsequently, as the typhoon moved northward, the stronger northerly wind further broadened the source areas of
385 the O₃ in the GBA (Figure S7). The major contributor of Day-2 and earlier periods' emissions changed to pollutants
386 from the EC and NCP regions. The pollutants emitted earlier than 2 days ago from the EC had an important
387 contribution, which accounted for about 12%. Furthermore, the pollutants emitted 3 days ago from the NCP can
388 also have a noticeable impact on O₃ over the GBA from July 28th-30th, which can be up to 10%. Therefore, to
389 prevent the occurrence of this pollution, emission control measures should be implemented in a broader region
390 and continuously enforced, as this pollution episode lasted longer compared to the other three cases.

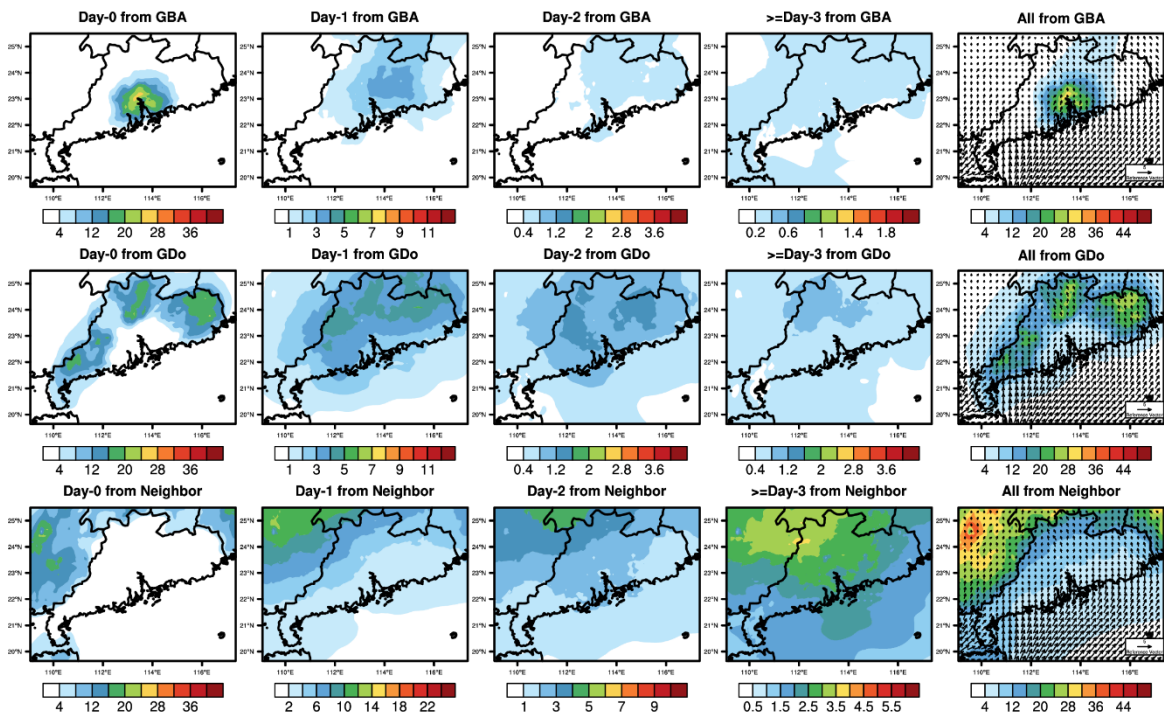
391 Figure S8 shows the time series of the contributions from different source areas and precursor emission periods
392 to the hourly average O₃ concentration in the GF region and HK city. GF region is located at the inland of the
393 GBA. It is the emission hotspot of the GBA with a higher O₃ concentration (Chen et al., 2022a). HK city is located
394 at the mouth of the PRD. According to previous source apportionment studies (Li et al., 2012, 2013), the pollution
395 in HK city is more attributed to the emissions outside the GBA compared to the other cities of the GBA. Regarding
396 the O₃ in the GF region, the Day-0 emission was usually contributed by both local emission and regional transport
397 within the GBA, with similar contributions. The major source areas of the Day-2 to Day-4 emissions contributing
398 to O₃ in the GF in different episodic cases varied similarly to those contributing to the hourly average O₃ in the
399 GBA. Generally, the influence of local and GBA regional pollutants on O₃ in the GF region diminished rapidly
400 within 1 day. However, the regional emission can still have an important contribution in the episodic case with
401 southerly winds, such as the 24th -25th July (about 26%) in the Ep2 and 23rd -25th (about 15%) in the Ep4. For the
402 O₃ in HK city, the local emission amount is low, and its impact was also limited to the current day. In addition,
403 the O₃ in HK city was also susceptible to the impact of pollutants from the ocean but less from the GBA regional
404 emissions. During the Ep1 periods, it was observed that the contribution of the GBA regional sources largely
405 increased in the Day-0 emission as the prevailing wind direction shifted to the north. On the other hand,
406 neighboring provinces' emissions dominated the contributions of emissions from Day-1 to Day-3. Unlike the GF
407 region, the influence of EC emissions on the O₃ in HK was also limited in Ep1. Similar conclusions can be drawn
408 for the evolution of the spatiotemporal contribution of emissions in Ep3. As discussed above, the O₃ pollution in
409 Ep2 was mainly driven by local emissions. Thus, the O₃ concentration in HK city, located in the upwind region
410 with fewer local emissions, was much lower than the O₃ concentration in the GF region. In Ep4, same as the GBA
411 average and GF region, the impact of pollutants from EC and NCP became important in the Day-2 and Day-3
412 emissions, which can contribute up to 20% of O₃. These results indicate that although O₃ is usually considered a
413 regional pollution problem, it's necessary to consider the local characteristics of different sub-regions when
414 making more specific prevention and control policies.



415

416 Figure 5. Time series of contributions from different source areas and emitting periods to the O₃ concentrations in
 417 the GBA. (*GDo* represents areas outside the GBA region but within Guangdong province. *Neighbor* represents
 418 the provinces around Guangdong province. *Other 1* represents ocean and other countries. *Other 2* represents other
 419 area within the mainland China in the simulation domain.)

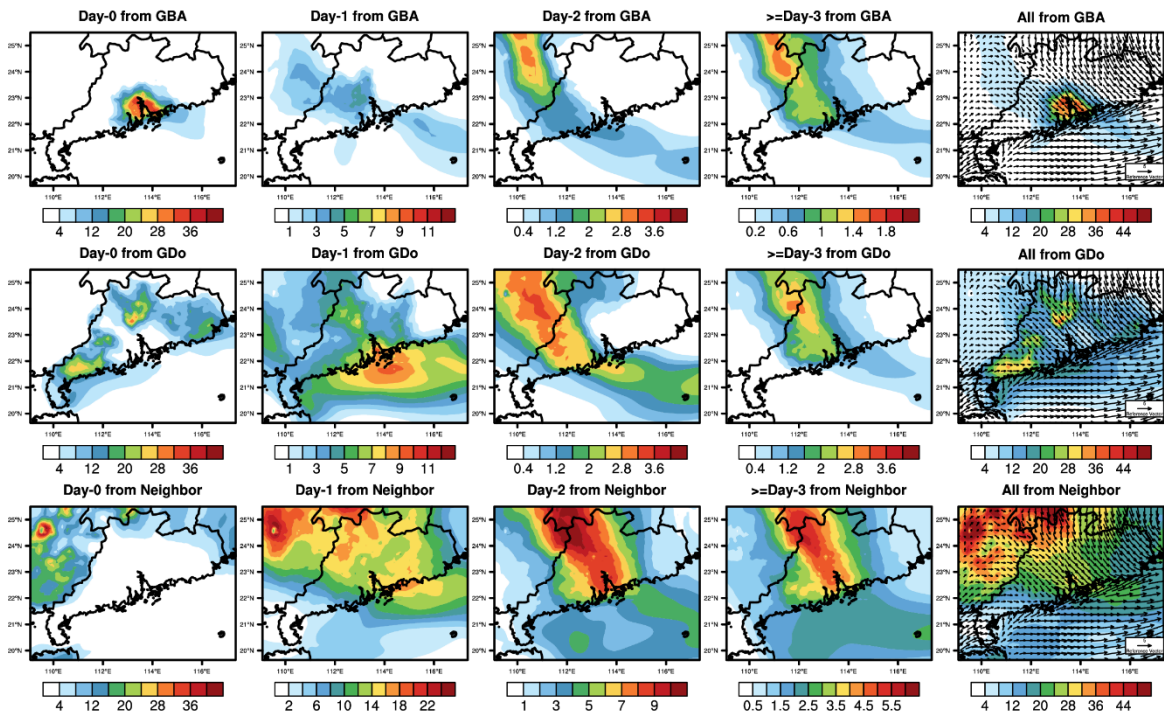
Monthly Average O₃ concentration (ppb)



420

421 Figure 6. Spatial distribution of monthly average O₃ concentration between 9:00-17:00 (Local time) contributed
 422 by emission of GBA, other regions within Guangdong province (GDo), and neighboring provinces (Neighbor)
 423 from various periods. (Unit: ppb. Due to the large variation of contribution, the colorbar range of each sub-figure
 424 is different)

Average O₃ concentration during 7-10 July (ppb)

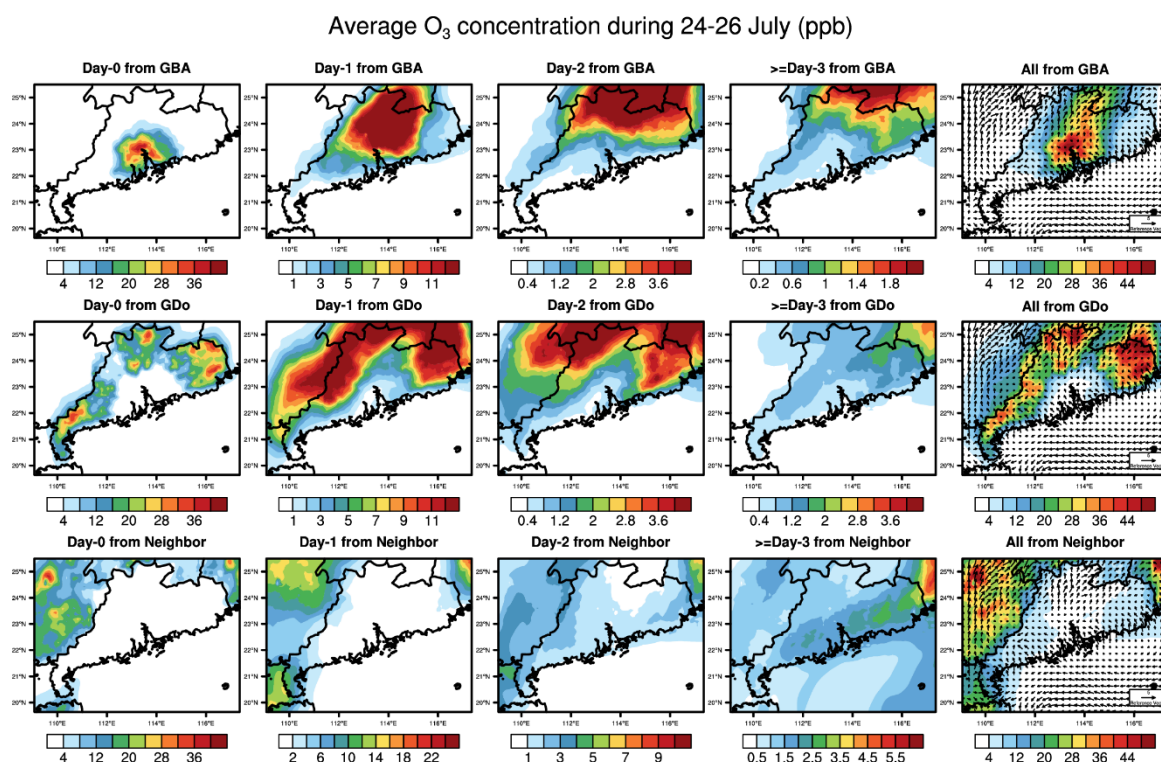


425

426

427

Figure 7. Same as Figure 6, but for the period of 7th-10th July 2016



428

429

Figure 8. Same as Figure 6, but for the period of 24th-26th July 2016.

430

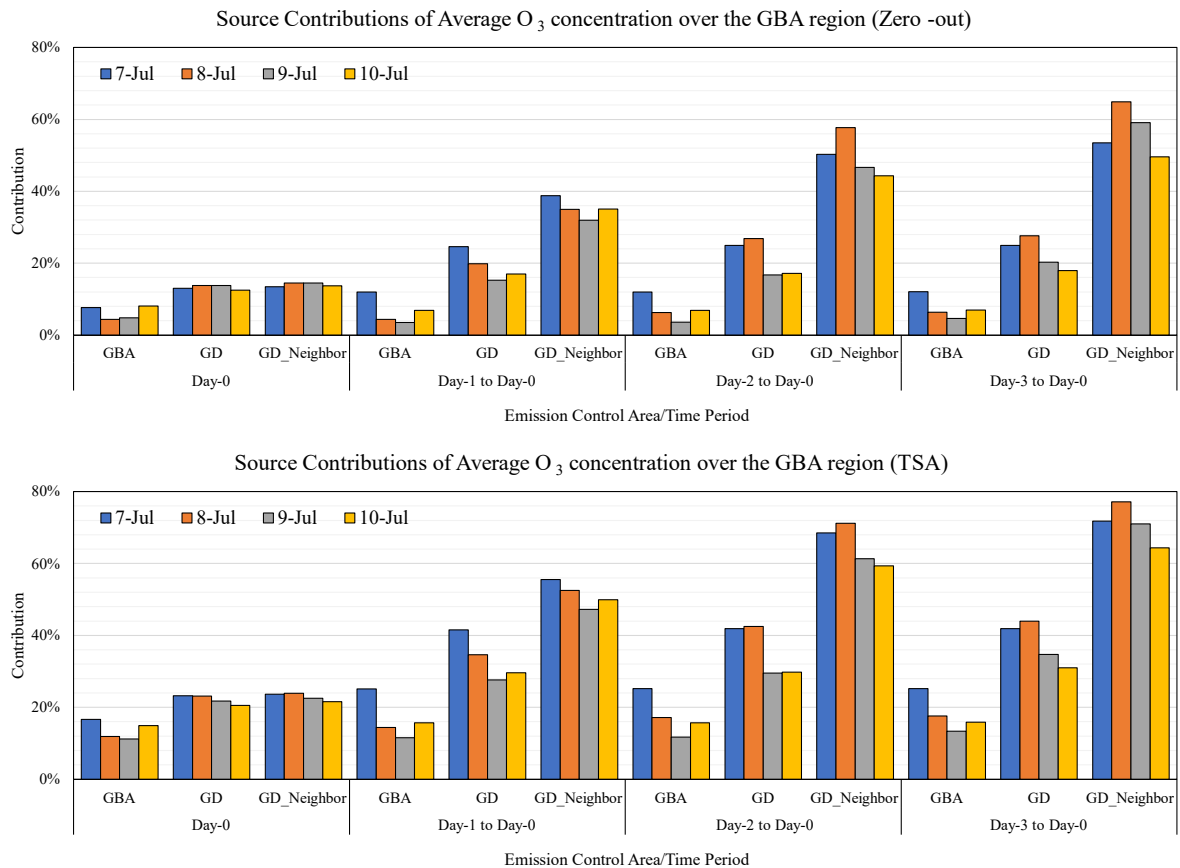
431 3.4 Verification of the TSA by comparing to Zero-out Experiments

432 Here, the emission zero-out sensitivity experiments, another commonly used method for source apportionment,
 433 were also conducted to evaluate the results from the TSA method. The zero-out method needs to conduct two sets
 434 of simulations, including the control run and the zero-out run. In the control run, the simulations were conducted
 435 using the complete emissions. In the zero-out runs, the simulations were conducted with the emissions that specific
 436 period and area were removed. Subsequently, the contribution of the specific source area and source time was
 437 derived by calculating the difference between the control and zero-out simulations. For each target date, three
 438 types of emission area controls were implemented: Type 1 involved the GBA region alone (GBA); Type 2 included
 439 the emission within Guangdong province (GD, namely GBA+GDo); and Type 3 expanded to encompass the
 440 emission within Guangdong province and neighbouring provinces (GD_Neighbor, namely GBA + GDo +
 441 Neighbor). The emission control period was set as continuous control beginning from the current day, which is
 442 also the target day (Day-0), from 1 day ago (Day-1), from 2 days ago (Day-2) and from 3 days ago (Day-3),
 443 respectively. The zero-out experiments were carried out for the periods between 7th and 10th July (Typhoon case)
 444 and between 24th and 26th (Sub-tropical high case). More configurations can be found in Tables S4- S5.

445 From the result of zero-out experiments (Fig.9 and Fig.S9), it can be seen that, for the typhoon case (Fig.9), when
 446 only controlling the emission within the GBA, there is little difference between results of controlling emissions 1
 447 day and 3 days in advance. This is consistent with the TSA result that the influence of the emission within the
 448 GBA is usually limited to 2 days. Controlling emissions 1 day in advance in GD yields better results compared to
 449 solely controlling emissions within the GBA. There is less variation of the O₃ concentration when controlling the
 450 emission within GD 2 or 3 days in advance. Meanwhile, regarding only controlling emissions on Day-0, there is
 451 limited improvement in controlling the emission for a larger area (GD and GD_Neighbor) than solely within the
 452 GBA. This result aligns with the TSA result that the pollutants from neighboring provinces took effect on the O₃
 453 over the GBA region at least 1 day later. Joint control from Guangdong and neighboring province has a better
 454 optimal effect in the simulations conducted from Day-2 to Day-0 and Day-3 to Day-0. The difference between
 455 GD_Neighbor and the GD result is more pronounced in these simulations, indicating that it's more effective to
 456 implement joint control within other provinces 2-3 days in advance.

457 For the sub-tropical high case (Fig.S9), whatever controlling the emissions on the current day or 2 days ahead, the
 458 effect of solely controlling emissions within the GBA is similar to those of joint control in a larger area (GD and
 459 GD_Neighbor). It supports our previous conclusion that the pollution is mainly contributed by the local sources.
 460 Additionally, there is limited optimization effect to control the emission 2-3 days in advance than controlling 1
 461 day in advance. To alleviate this ozone pollution, controlling the local emission in the short term should be
 462 effective. Although the contribution discrepancies between the source contribution (%) calculated from the zero-
 463 out method and those obtained from the TSA method can reach 20%, which is due to the non-linear chemistry
 464 relationship between ozone and its precursors, as well as the differences in the methodology (Kwok et al., 2015;
 465 Clappier et al., 2017), similar relationships between source area/time and receptor can be drawn. These results
 466 also support the validity of the TSA approach.

467



468

469 Figure 9. The contribution of different source areas and time periods to the O₃ concentration over the GBA in the
 470 typhoon case using the zero-out and TSA methods. (Different colors represent different target dates; Upper: Zero-
 471 out; Bottom: TSA)

472

473 3.5 Discussion

474 Previous studies mainly focused on exploring the contribution and control of various source areas and categories
 475 on O₃ over the GBA. The analysis in this study illustrated that there could be a larger difference between the
 476 temporal contribution of emissions to the O₃ pollution over the GBA under different weather patterns. This finding
 477 emphasizes the importance of understanding the contribution of pollutants from different emission periods and
 478 identifying the major periods, particularly in episodic cases, for effective policymaking in pollution control. In
 479 contrast to the zero-out method, which requires multiple simulations, our approach provides a comprehensive
 480 overview of source contributions within a single simulation. This method is suited for applications involving more
 481 potential sources as it saves computation costs.

482 In addition, meteorological conditions play an important role in affecting the effectiveness of the emission control
483 area and period. The results here suggest that the approach of typhoons usually strengthens the cross-region
484 transportation of pollutants to the GBA. Therefore, cross-province collaboration and control should be
485 implemented at least 2-3 days ahead when the typhoon is predicted. The information obtained from the TSA results
486 can contribute to the establishment of an early warning and rapid response system. It could help to facilitate
487 collaboration, considering estimated timelines and the cost implications associated with emission reduction efforts,
488 aiming to achieve a balanced outcome across regions. In contrast, local emission control within 2 days is more
489 effective when the GBA is under the influence of a high-pressure system. The primary focus for emission control
490 measures should be on local vehicles and industries, as they are the major contributors of NO_x and VOCs (Bian
491 et al., 2019; Li et al., 2019). Implementing measures such as traffic restrictions based on even- and odd-numbered
492 license plates and temporary reduction of emissions from industries can be effective strategies to target these
493 sources in advance. Our findings emphasize the importance of considering the impact of meteorological
494 conditions when implementing control measures in advance. Here, our study primarily focuses on the summer
495 season, which has been identified as the O₃ pollution period in the GBA (Gao et al., 2018; Li et al., 2022).
496 Typhoons and subtropical high-pressure systems are two significant weather patterns closely linked with O₃
497 pollution events in Southern China (Wang et al., 2017; Ouyang et al., 2022). The trajectories of typhoons in
498 episodes 1 and 3 (Figure S3) are similar to one of the typical typhoon pathways, often coinciding with O₃ pollution
499 events in the GBA (Qu et al., 2021; Wang et al., 2022a). Meanwhile, the high 2-m temperature and low 2-m
500 relative humidity over the GBA can be observed during the O₃ episodes (Figure S10-S11). The prevailing wind
501 across the GBA in the typhoon and sub-tropical high-pressure cases is northerly and southerly, respectively
502 (Figures S12). Overall, the weather conditions observed in the selected cases of this study are similar to those
503 reported in other O₃ pollution studies in this region (Qu et al., 2021 Ouyang et al., 2022; Wang et al., 2022).
504 Nevertheless, it is crucial to underscore that the spatial-temporal source contribution may vary in O₃ pollutions
505 even under similar meteorological conditions. For instance, the change of typhoon position and intensity could
506 influence the large-scale circulation and precursor emission (Zhan et al., 2020; Wang et al., 2022a). Therefore, it
507 is imperative to undertake further investigations and comparative studies on more similar O₃ events over the GBA
508 under the influence of typhoons and subtropical high-pressures in the future, which will contribute to attaining
509 more widely applicable findings and offer valuable insights for developing emission control strategies.
510 Additionally, the spatial-temporal influence of emission to O₃ over the GBA under other unfavourable conditions
511 and seasons is also essential to further explore through the TSA method, which helps to gain a more comprehensive
512 understanding of when and where the O₃ over the GBA comes from.

513 In the context of climate change, the occurrence of extreme weather, such as extreme heatwaves (Coffel et al.,
514 2018; Dong et al., 2023), is expected to become more frequent. These events will significantly impact the sources
515 and sinks of pollutants through various physical and chemical processes. At the same time, governments in
516 different countries will implement various emission control strategies in response to climate change, such as
517 carbon neutrality (Liu et al., 2021; Zhang et al., 2021), which will also alter the emission structure. How these
518 extreme weather events and control measures influence the temporal characterization of sources, the formation of
519 air pollution, and the spatial-temporal contribution of emissions from different countries, as well as their
520 interactions, are also worth further investigation in the future. Such investigations can foster mutual cooperation
521 among nations to collectively address environmental challenges.

522 However, it should be noted that the numerical model source apportionment results are usually influenced by the
523 uncertainties of the emission inventory as most of the emission inventories are constructed by the bottom-up
524 method and cannot be updated in a timely manner. With the increasing availability of different types of
525 observations, including surface monitoring and satellite remote sensing data, different top-down methods such as
526 data assimilation (East et al., 2022) and machine learning (Chen et al., 2023) have been applied to integrate
527 observations and optimize the emissions. These methods should be implemented to update the emission inventory.
528 Meanwhile, the air quality model results are also sensitive to the uncertainty in the weather forecast, potentially
529 leading to variations in source apportionment results. To alleviate the impact of weather forecast uncertainty,
530 different methods, such as ensemble simulation (Gilliam et al., 2015), data assimilation for the meteorological
531 field simulation (Kwon et al., 2018), and machine learning method (Scher et al., 2018; Cho et al., 2020), should
532 be applied to enhance the accuracy of meteorological field simulations.

533

534

535 **4. Conclusion**

536 In this study, we applied the CAMx-TSA method to analyze the spatial and temporal contribution of different
537 sources to the O₃ pollution in the GBA during summer. The result shows that the O₃ over the GBA in summer is
538 mainly contributed by the pollutants from local emissions, followed by pollutants originating from other regions
539 within Guangdong province and neighbouring provinces. The O₃ formation is predominantly attributed to
540 pollutants emitted within a 3-day period, accounting for over 70% of the total contribution. During the O₃ episodes,
541 when the typhoon moved from the eastern Philippine Sea towards southern China, the prevailing wind shifted
542 from south to north over the GBA. This facilitated the transport of pollutants from GDo and neighbouring provinces
543 to the GBA, resulting in an increase in O₃ concentrations. The pollutants emitted 3 days ago still have a significant
544 contribution. When the typhoon remained near the sea areas east of Taiwan province and moved northward, under
545 the continuous influence of northerly wind, the emissions from eastern China, even the North China Plain from 3
546 days ago can also have a noticeable impact on O₃ over the GBA. In contrast, when the GBA was mainly under the
547 control of the sub-tropical high-pressure system, the ozone pollution was mainly caused by the local pollutants
548 within the current 2 days. The results indicated that implementing joint emission control measures with other
549 provinces 2-3 days in advance is more effective for preventing the O₃ pollution in the GBA when the typhoon is
550 approaching southern China. On the other hand, it's more efficient to pay more attention to local source control
551 within 2 days when the GBA is under the control of the high-pressure system.

552 Here, different surrounding provinces were categorized as one source area here to save computation resource for
553 more potential source investigation. As the neighbouring province was illustrated as a major contributor to the O₃
554 in the GBA, it is necessary to further divided this source into several sub-source areas and explore their individual
555 impact in future work. Meanwhile, our preliminary findings indicate that pollutants emitted more than three days
556 prior can still have a considerable impact on the O₃ levels in the GBA. As a result, it would be valuable to conduct
557 source apportionment analyses with finer source areas and earlier source periods for O₃ pollution in different cities
558 within the GBA. This further investigation would provide deeper insights into the unique O₃ pollution
559 characteristics of each city. In addition, individual source categories were not separated in this study, mainly due
560 to the application of different emission inventories with different source category classifications, making it
561 difficult to combine them. It is important to note that each source category has its own characteristic temporal
562 profile, which can have different temporal impacts on O₃ concentrations. Therefore, the temporal contribution of
563 various source categories, including anthropogenic and biogenic emissions, should be also considered in future
564 work. These works can provide more spatial and temporal information of O₃ source over the GBA, enabling local
565 governments to design and implement more targeted control measures more effectively and promptly.

566

567 **Code and Data availability**

568 Hourly O₃ observation data were released by the China National Environmental Monitoring Centre
569 (<http://www.cnemc.cn/en>, last access 24 December; CNEMC, 2023) and the Hong Kong Environmental
570 Protection Department (<https://cd.epic.epd.gov.hk/EPICDI/air/station/?lang=en>, last access 24 December 2023;
571 HKEPD, 2023). The CAMx model code is freely available via <https://www.camx.com/download/>, last access 24
572 December, 2023). The ECMWF Reanalysis v5 (ERA5) data was downloaded from
573 <https://www.ecmwf.int/en/forecasts/dataset/ecmwf-reanalysis-v5>, last access 17 May 2024; ERA5, 2024)

574

575 **Author contribution**

576 CY, LX, and JF designed the research. CY contributed to model development, simulation and data analysis. LX
577 and JF contributed to the result discussion. CY prepared the manuscript with contributions from all co-authors.

578

579 **Competing interests**

580 The authors declare that they have no conflict of interest.

581

582 **Acknowledgements**

583 This work was supported by the Research Grants Council of Hong Kong Government (C6026-22GF) and the
584 Improvement on Competitiveness in Hiring New Faculties Funding Scheme of CUHK (No. 4937115)

585

586 **References**

587 Bian, Y., Huang, Z., Ou, J., Zhong, Z., Xu, Y., Zhang, Z., Xiao, X., Ye, X., Wu, Y., Yin, X., Li, C., Chen, L., Shao,
588 M., and Zheng, J.: Evolution of anthropogenic air pollutant emissions in Guangdong Province, China, from 2006
589 to 2015, *Atmospheric Chemistry and Physics*, 19, 11701-11719, 10.5194/acp-19-11701-2019, 2019.

590 Cao, M., Fan, S., Jin, C., Cai, Q., and He, Y.: O₃ pollution characteristics, weather classifications and local
591 meteorological conditions in Guangdong from 2015 to 2020, *Acta Scientiae Circumstantiae*, 43, 19-31,
592 10.13671/j.hjkxxb.2022.0416, 2023. (in Chinese)

593 Cao, T., Wang, H., Li, L., Lu, X., Liu, Y., and Fan, S.: Fast spreading of surface ozone in both temporal and spatial
594 scale in Pearl River Delta, *Journal of Environmental Sciences*, 137, 540-552, 10.1016/j.jes.2023.02.025, 2024.

595 Chen, W., Chen, Y., Chu, Y., Zhang, J., Xian, C., Lin, C., Fung, Z., and Lu, X.: Numerical simulation of ozone
596 source characteristics in the Pearl River Delta region, *Acta Scientiae Circumstantiae*, 42, 293-308,
597 10.13671/j.hjkxxb.2021.0328, 2022a. (in Chinese)

598 Chen, X., Wang, N., Wang, G., Wang, Z., Chen, H., Cheng, C., Li, M., Zheng, L., Wu, L., Zhang, Q., Tang, M.,
599 Huang, B., Wang, X., and Zhou, Z.: The Influence of Synoptic Weather Patterns on Spatiotemporal Characteristics
600 of Ozone Pollution Across Pearl River Delta of Southern China, *Journal of Geophysical Research: Atmospheres*,
601 127, 10.1029/2022jd037121, 2022b.

602 Chen, Y., Fung, J. C. H., Huang, Y., Lu, X., Wang, Z., Louie, P. K. K., Chen, W., Yu, C. W., Yu, R., and Lau, A. K.
603 H.: Temporal Source Apportionment of PM_{2.5} Over the Pearl River Delta Region in Southern China, *Journal of*
604 *Geophysical Research: Atmospheres*, 127, 10.1029/2021jd035271, 2022c.

605 Chen, Y., Fung, J. C. H., Yuan, D., Chen, W., Fung, T., and Lu, X.: Development of an integrated machine-learning
606 and data assimilation framework for NO_x emission inversion, *Science of The Total Environment*, 871,
607 10.1016/j.scitotenv.2023.161951, 2023.

608 Cho, D., Yoo, C., Im, J., and Cha, D. H.: Comparative Assessment of Various Machine Learning -Based Bias
609 Correction Methods for Numerical Weather Prediction Model Forecasts of Extreme Air Temperatures in Urban
610 Areas, *Earth and Space Science*, 7, 10.1029/2019ea000740, 2020.

611 Clappier, A., Belis, C. A., Pernigotti, D., and Thunis, P.: Source apportionment and sensitivity analysis: two
612 methodologies with two different purposes, *Geoscientific Model Development*, 10, 4245-4256, 10.5194/gmd-10-
613 4245-2017, 2017.

614 CNEMC: China National Environmental Monitoring Centre: Real-time National Air Quality,
615 <http://www.cnemc.cn/en>, last access: 24 December 2023.

616 Coffel, E. D., Horton, R. M., and de Sherbinin, A.: Temperature and humidity based projections of a rapid rise in
617 global heat stress exposure during the 21st century, *Environmental Research Letters*, 13, 10.1088/1748-
618 9326/aaa00e, 2018.

619 Deng, T., Wang, T., Wang, S., Zou, Y., Yin, C., Li, F., Liu, L., Wang, N., Song, L., Wu, C., and Wu, D.: Impact of
620 typhoon periphery on high ozone and high aerosol pollution in the Pearl River Delta region, *Science of The Total*
621 *Environment*, 668, 617-630, 10.1016/j.scitotenv.2019.02.450, 2019.

622 Dong, W., Jia, X., Qian, Q., and Li, X.: Rapid Acceleration of Dangerous Compound Heatwaves and Their Impacts
623 in a Warmer China, *Geophysical Research Letters*, 50, 10.1029/2023gl104850, 2023.

624 East, J. D., Henderson, B. H., Napelenok, S. L., Koplitz, S. N., Sarwar, G., Gilliam, R., Lenzen, A., Tong, D. Q.,
625 Pierce, R. B., and Garcia-Menendez, F.: Inferring and evaluating satellite-based constraints on NO_x emissions

626 estimates in air quality simulations, *Atmospheric Chemistry and Physics*, 22, 15981-16001, 10.5194/acp-22-
627 15981-2022, 2022.

628 Emery, C., Tai, E., and Yarwood, G.: Enhanced meteorological modeling and performance evaluation for two
629 Texas ozone episodes, Prepared for the Texas natural resource conservation commission, by ENVIRON
630 International Corporation, 2001.

631 EPA, U.: Guidance on the use of models and other analyses for demonstrating attainment of air quality goals for
632 ozone, PM_{2.5}, and regional haze, Technical Support Document, 2007.

633 ERA5, ECMWF Reanalysis v5 data, <https://www.ecmwf.int/en/forecasts/dataset/ecmwf-reanalysis-v5>, last access
634 17 May 2024; ERA5, 2024

635 Fang, T., Zhu, Y., Wang, S., Xing, J., Zhao, B., Fan, S., Li, M., Yang, W., Chen, Y., and Huang, R.: Source impact
636 and contribution analysis of ambient ozone using multi-modeling approaches over the Pearl River Delta region,
637 China, *Environmental Pollution*, 289, 10.1016/j.envpol.2021.117860, 2021.

638 Feng, X., Guo, J., Wang, Z., Gu, D., Ho, K.-F., Chen, Y., Liao, K., Cheung, V. T. F., Louie, P. K. K., Leung, K. K.
639 M., Yu, J. Z., Fung, J. C. H., and Lau, A. K. H.: Investigation of the multi-year trend of surface ozone and ozone-
640 precursor relationship in Hong Kong, *Atmospheric Environment*, 315, 10.1016/j.atmosenv.2023.120139, 2023.

641 Gao, X., Deng, X., Tan, H., Wang, C., Wang, N., and Yue, D.: Characteristics and analysis on regional pollution
642 process and circulation weather types over Guangdong Province, *Acta Scientiae Circumstantiae*, 38, 1708-1716,
643 10.13671/j.hjkxxb.2017.0473, 2018. (in Chinese)

644 Gilliam, R. C., Hogrefe, C., Godowitch, J. M., Napelenok, S., Mathur, R., and Rao, S. T.: Impact of inherent
645 meteorology uncertainty on air quality model predictions, *Journal of Geophysical Research: Atmospheres*, 120,
646 10.1002/2015jd023674, 2015.

647 Gong, C., Liao, H., Yue, X., Ma, Y., and Lei, Y.: Impacts of Ozone-Vegetation Interactions on Ozone Pollution
648 Episodes in North China and the Yangtze River Delta, *Geophysical Research Letters*, 48, 10.1029/2021gl093814,
649 2021.

650 Gong, S., Zhang, L., Liu, C., Lu, S., Pan, W., and Zhang, Y.: Multi-scale analysis of the impacts of meteorology
651 and emissions on PM_{2.5} and O₃ trends at various regions in China from 2013 to 2020 2. Key weather elements and
652 emissions, *Science of The Total Environment*, 824, 10.1016/j.scitotenv.2022.153847, 2022.

653 Han, H., Liu, J., Shu, L., Wang, T., and Yuan, H.: Local and synoptic meteorological influences on daily variability
654 in summertime surface ozone in eastern China, *Atmospheric Chemistry and Physics*, 20, 203-222, 10.5194/acp-
655 20-203-2020, 2020.

656 He, Z., Wang, X., Ling, Z., Zhao, J., Guo, H., Shao, M., and Wang, Z.: Contributions of different anthropogenic
657 volatile organic compound sources to ozone formation at a receptor site in the Pearl River Delta region and its
658 policy implications, *Atmospheric Chemistry and Physics*, 19, 8801-8816, 10.5194/acp-19-8801-2019, 2019.

659 HKPD, Hong Kong Air Quality Data, <https://cd.epic.epd.gov.hk/EPICDI/air/station/?lang=en>, last access: 24
660 December 2023)

661 Kwok, R., Baker, K., Napelenok, S., and Tonnesen, G.: Photochemical grid model implementation and application
662 of VOC, NO_x, and O₃ source apportionment, *Geoscientific Model Development*, 8, 99-114, 2015.

663 Kwon, I.-H., English, S., Bell, W., Potthast, R., Collard, A., and Ruston, B.: Assessment of Progress and Status of
664 Data Assimilation in Numerical Weather Prediction, *Bulletin of the American Meteorological Society*, 99, ES75-
665 ES79, 10.1175/bams-d-17-0266.1, 2018.

666 Li, M., Liu, H., Geng, G., Hong, C., Liu, F., Song, Y., Tong, D., Zheng, B., Cui, H., Man, H., Zhang, Q., and He,
667 K.: Anthropogenic emission inventories in China: a review, *National Science Review*, 4, 834-866,
668 10.1093/nsr/nwx150, 2017.

669 Li, M., Zhang, Q., Zheng, B., Tong, D., Lei, Y., Liu, F., Hong, C., Kang, S., Yan, L., Zhang, Y., Bo, Y., Su, H.,
670 Cheng, Y., and He, K.: Persistent growth of anthropogenic non-methane volatile organic compound (NMVOC)

671 emissions in China during 1990–2017: drivers, speciation and ozone formation potential, *Atmospheric Chemistry*
672 *and Physics*, 19, 8897-8913, 10.5194/acp-19-8897-2019, 2019.

673 Li, T., Chen, J., Weng, J., Shen, J., and Gong, Y.: Ozone pollution synoptic patterns and their variation
674 characteristics in Guangdong Province, *China Environmental Science*, 42, 2015-2024, 10.19674/j.cnki.issn1000-
675 6923.2022.0102, 2022. (in Chinese)

676 Li, Y., Lau, A. K. H., Fung, J. C. H., Zheng, J. Y., Zhong, L. J., and Louie, P. K. K.: Ozone source apportionment
677 (OSAT) to differentiate local regional and super-regional source contributions in the Pearl River Delta region,
678 China, *Journal of Geophysical Research: Atmospheres*, 117, 10.1029/2011jd017340, 2012.

679 Li, Y., Lau, A. K. H., Fung, J. C. H., Ma, H., and Tse, Y.: Systematic evaluation of ozone control policies using an
680 Ozone Source Apportionment method, *Atmospheric Environment*, 76, 136-146, 10.1016/j.atmosenv.2013.02.033,
681 2013.

682 Li, Y., Zhao, X., Deng, X., and Gao, J.: The impact of peripheral circulation characteristics of typhoon on sustained
683 ozone episodes over the Pearl River Delta region, China, *Atmospheric Chemistry and Physics*, 22, 3861-3873,
684 10.5194/acp-22-3861-2022, 2022.

685 Lin, X., Yuan, Z., Yang, L., Luo, H., and Li, W.: Impact of Extreme Meteorological Events on Ozone in the Pearl
686 River Delta, China, *Aerosol and Air Quality Research*, 19, 1307-1324, 10.4209/aaqr.2019.01.0027, 2019.

687 Liu, H., Zhang, M., and Han, X.: A review of surface ozone source apportionment in China, *Atmospheric and*
688 *Oceanic Science Letters*, 13, 470-484, 10.1080/16742834.2020.1768025, 2020a.

689 Liu, Y. and Wang, T.: Worsening urban ozone pollution in China from 2013 to 2017 – Part 1: The complex and
690 varying roles of meteorology, *Atmospheric Chemistry and Physics*, 20, 6305-6321, 10.5194/acp-20-6305-2020,
691 2020b.

692 Liu, Y., Geng, G., Cheng, J., Liu, Y., Xiao, Q., Liu, L., Shi, Q., Tong, D., He, K., and Zhang, Q.: Drivers of
693 Increasing Ozone during the Two Phases of Clean Air Actions in China 2013–2020, *Environmental Science &*
694 *Technology*, 57, 8954-8964, 10.1021/acs.est.3c00054, 2023.

695 Liu, Z., Deng, Z., He, G., Wang, H., Zhang, X., Lin, J., Qi, Y., and Liang, X.: Challenges and opportunities for
696 carbon neutrality in China, *Nature Reviews Earth & Environment*, 3, 141-155, 10.1038/s43017-021-00244-x,
697 2021.

698 Lu, X., Yao, T., Li, Y., Fung, J. C. H., and Lau, A. K. H.: Source apportionment and health effect of NO_x over the
699 Pearl River Delta region in southern China, *Environmental Pollution*, 212, 135-146,
700 10.1016/j.envpol.2016.01.056, 2016.

701 Lu, X., Zhang, L., and Shen, L.: Meteorology and Climate Influences on Tropospheric Ozone: a Review of Natural
702 Sources, Chemistry, and Transport Patterns, *Current Pollution Reports*, 5, 238-260, 10.1007/s40726-019-00118-
703 3, 2019.

704 Maji, K. J., Ye, W.-F., Arora, M., and Nagendra, S. M. S.: Ozone pollution in Chinese cities: Assessment of
705 seasonal variation, health effects and economic burden, *Environmental Pollution*, 247, 792-801,
706 10.1016/j.envpol.2019.01.049, 2019.

707 Ouyang, S., Deng, T., Liu, R., Chen, J., He, G., Leung, J. C.-H., Wang, N., and Liu, S. C.: Impact of a subtropical
708 high and a typhoon on a severe ozone pollution episode in the Pearl River Delta, China, *Atmospheric Chemistry*
709 *and Physics*, 22, 10751-10767, 10.5194/acp-22-10751-2022, 2022.

710 Qu, K., Wang, X., Yan, Y., Shen, J., Xiao, T., Dong, H., Zeng, L., and Zhang, Y.: A comparative study to reveal
711 the influence of typhoons on the transport, production and accumulation of O₃ in the Pearl River Delta, China,
712 *Atmospheric Chemistry and Physics*, 21, 11593-11612, 10.5194/acp-21-11593-2021, 2021.

713 Sahu, S. K., Liu, S., Liu, S., Ding, D., and Xing, J.: Ozone pollution in China: Background and transboundary
714 contributions to ozone concentration & related health effects across the country, *Science of The Total Environment*,
715 761, 10.1016/j.scitotenv.2020.144131, 2021.

716 Scher, S. and Messori, G.: Predicting weather forecast uncertainty with machine learning, *Quarterly Journal of*
717 *the Royal Meteorological Society*, 144, 2830-2841, 10.1002/qj.3410, 2018.

718 Wang, N., Huang, X., Xu, J., Wang, T., Tan, Z.-m., and Ding, A.: Typhoon-boosted biogenic emission aggravates
719 cross-regional ozone pollution in China, *Science Advances*, 8, eabl6166, 2022a.

720 Wang, T., Xue, L., Brimblecombe, P., Lam, Y. F., Li, L., and Zhang, L.: Ozone pollution in China: A review of
721 concentrations, meteorological influences, chemical precursors, and effects, *Science of The Total Environment*,
722 575, 1582-1596, 10.1016/j.scitotenv.2016.10.081, 2017.

723 Wang, T., Xue, L., Feng, Z., Dai, J., Zhang, Y., and Tan, Y.: Ground-level ozone pollution in China: a synthesis of
724 recent findings on influencing factors and impacts, *Environmental Research Letters*, 17, 10.1088/1748-
725 9326/ac69fe, 2022b.

726 Wang, Y., Wild, O., Ashworth, K., Chen, X., Wu, Q., Qi, Y., and Wang, Z.: Reductions in crop yields across China
727 from elevated ozone, *Environmental Pollution*, 292, 10.1016/j.envpol.2021.118218, 2022c.

728 Wang, W., Parrish, D. D., Wang, S., Bao, F., Ni, R., Li, X., Yang, S., Wang, H., Cheng, Y., and Su, H.: Long-term
729 trend of ozone pollution in China during 2014–2020: distinct seasonal and spatial characteristics and ozone
730 sensitivity, *Atmospheric Chemistry and Physics*, 22, 8935-8949, 10.5194/acp-22-8935-2022, 2022d.

731 Wu, Y., Chen, W., You, Y., Xie, Q., Jia, S., and Wang, X.: Quantitative impacts of vertical transport on the long-
732 term trend of nocturnal ozone increase over the Pearl River Delta region during 2006–2019, *Atmospheric*
733 *Chemistry and Physics*, 23, 453-469, 10.5194/acp-23-453-2023, 2023.

734 Xie, X., Shi, Z., Ying, Q., Zhang, H., and Hu, J.: Age-Resolved Source and Region Contributions to Fine
735 Particulate Matter During an Extreme Haze Episode in China, *Geophysical Research Letters*, 48,
736 10.1029/2021gl095388, 2021.

737 Xie, X., Hu, J., Qin, M., Guo, S., Hu, M., Ji, D., Wang, H., Lou, S., Huang, C., Liu, C., Zhang, H., Ying, Q., Liao,
738 H., and Zhang, Y.: Evolution of atmospheric age of particles and its implications for the formation of a severe
739 haze event in eastern China, *Atmospheric Chemistry and Physics*, 23, 10563-10578, 10.5194/acp-23-10563-2023,
740 2023.

741 Xu, J., Zhao, Z., Wu, Y., Zhang, Y., Wang, Y., Su, B., Liang, Y., Hu, T., and Liu, R.: Impacts of Meteorological
742 Conditions on Autumn Surface Ozone During 2014–2020 in the Pearl River Delta, China, *Earth and Space Science*,
743 10, 10.1029/2022ea002742, 2023a.

744 Xu, Y., Shen, A., Jin, Y., Liu, Y., Lu, X., Fan, S., Hong, Y., and Fan, Q.: A quantitative assessment and process
745 analysis of the contribution from meteorological conditions in an O₃ pollution episode in Guangzhou, China,
746 *Atmospheric Environment*, 303, 10.1016/j.atmosenv.2023.119757, 2023b.

747 Yang, J. and Zhao, Y.: Performance and application of air quality models on ozone simulation in China – A review,
748 *Atmospheric Environment*, 293, 10.1016/j.atmosenv.2022.119446, 2023.

749 Yang, L., Luo, H., Yuan, Z., Zheng, J., Huang, Z., Li, C., Lin, X., Louie, P. K. K., Chen, D., and Bian, Y.:
750 Quantitative impacts of meteorology and precursor emission changes on the long-term trend of ambient ozone
751 over the Pearl River Delta, China, and implications for ozone control strategy, *Atmospheric Chemistry and Physics*,
752 19, 12901-12916, 10.5194/acp-19-12901-2019, 2019a.

753 Yang, W., Chen, H., Wang, W., Wu, J., Li, J., Wang, Z., Zheng, J., and Chen, D.: Modeling study of ozone source
754 apportionment over the Pearl River Delta in 2015, *Environmental Pollution*, 253, 393-402,
755 10.1016/j.envpol.2019.06.091, 2019b.

756 Yin, P., Chen, R., Wang, L., Meng, X., Liu, C., Niu, Y., Lin, Z., Liu, Y., Liu, J., Qi, J., You, J., Zhou, M., and Kan,
757 H.: Ambient Ozone Pollution and Daily Mortality: A Nationwide Study in 272 Chinese Cities, *Environmental*
758 *Health Perspectives*, 125, 10.1289/ehp1849, 2017.

759 Ying, Q., Zhang, J., Zhang, H., Hu, J., and Kleeman, M. J.: Atmospheric Age Distribution of Primary and
760 Secondary Inorganic Aerosols in a Polluted Atmosphere, *Environmental Science & Technology*, 55, 5668-5676,
761 10.1021/acs.est.0c07334, 2021.

762 Zeren, Y., Zhou, B., Zheng, Y., Jiang, F., Lyu, X., Xue, L., Wang, H., Liu, X., and Guo, H.: Does Ozone Pollution
763 Share the Same Formation Mechanisms in the Bay Areas of China?, *Environmental Science & Technology*, 56,
764 14326-14337, 10.1021/acs.est.2c05126, 2022.

765 Zhang, R. and Hanaoka, T.: Deployment of electric vehicles in China to meet the carbon neutral target by 2060:
766 Provincial disparities in energy systems, CO₂ emissions, and cost effectiveness, *Resources, Conservation and*
767 *Recycling*, 170, 10.1016/j.resconrec.2021.105622, 2021.

768 Zhan, C., Xie, M., Huang, C., Liu, J., Wang, T., Xu, M., Ma, C., Yu, J., Jiao, Y., Li, M., Li, S., Zhuang, B., Zhao,
769 M., and Nie, D.: Ozone affected by a succession of four landfall typhoons in the Yangtze River Delta, China:
770 major processes and health impacts, *Atmospheric Chemistry and Physics*, 20, 13781-13799, 10.5194/acp-20-
771 13781-2020, 2020.

772 Zheng, H., Kong, S., He, Y., Song, C., Cheng, Y., Yao, L., Chen, N., and Zhu, B.: Enhanced ozone pollution in the
773 summer of 2022 in China: The roles of meteorology and emission variations, *Atmospheric Environment*, 301,
774 10.1016/j.atmosenv.2023.119701, 2023.

775